Applied Catalysis B: Environmental 223 (2018) 154–166

Contents lists available at ScienceDirect

Applied Catalysis B: Environmental

journal homepage: www.elsevier.com/locate/apcatb

Influence of the preparation method on the activity of copper-manganese oxides for toluene total oxidation

Z. Ye[a,b], J.-M. Giraudon[a,*], N. Nuns[a], P. Simon[a], N. De Geyter[b], R. Morent[b], J.-F. Lamonier[a,*]

[a] Univ. Lille, CNRS, Centrale Lille, ENSCL, Univ. Artois, UMR 8181 – UCCS – Unité de Catalyse et Chimie du Solide, F-59000 Lille, France
[b] Ghent University, Faculty of Engineering, Department of Applied Physics, Research Unit Plasma Technology, Sint-Pietersnieuwstraat 41, 9000 Ghent, Belgium

ARTICLE INFO

Article history:
Received 29 November 2016
Received in revised form 12 June 2017
Accepted 23 June 2017
Available online 23 June 2017

Keywords:
VOC
Catalytic oxidation
Toluene
Copper-manganese oxide
Preparation method

ABSTRACT

Copper manganese oxides were prepared either by a co-precipitation method using metal nitrates as precursors, tetramethylammonium hydroxide (TMAH) as precipitant or by a redox-precipitation method using manganese acetate and copper nitrate as precursors, permanganate of potassium as oxidant. Copper manganese oxides synthesized by the redox method and calcined at 300 °C were also doped with Pt and Pd (0.5 wt%). The materials were characterized by ICP-OES, X-ray powder diffraction, N_2 adsorption/desorption analysis, temperature-programmed reduction, X-ray photoelectron spectroscopy and time-of-flight secondary-ion mass spectrometry. The catalyst properties were assessed in total oxidation of toluene and compared with those of the corresponding single oxides and of a commercial Hopcalite catalyst. Copper manganese oxides were proved to be more active than the single oxides whatever the method of preparation used. CuMnOx prepared via redox method were more active than the catalyst prepared by co-precipitation and compared favorably with the commercial Hopcalite. The overall characterization results revealed that the redox method can ensure a good dispersion of copper in close interaction with manganese preserving more active sites at the outermost layers of the catalyst in comparison with the catalyst obtained via co-precipitation. However all the catalysts deactivate to some extent at the earlier stages of the reaction before to reach a steady-state. For redox catalysts calcined at 300 °C, although the dispersion of trace amount of noble metals does not ensure a better activity, adding Pt allows to get a better resistance to deactivation. Additionally it is to be noticeable that the catalyst using redox-precipitation method calcined at 200 °C outperforms the commercial hopcalite overtime on stream.

1. Introduction

Most volatile organic compounds (VOCs) which are classified as major contributors to air pollution are harmful to the atmosphere and human health. They contribute as direct hazardous pollutants and indirectly as tropospheric ozone/photochemical smog precursors [1]. As a result, it is highly desired to control the emissions of VOCs. Among the various strategies for VOC elimination, catalytic oxidation is believed to be one of the most effective alternatives because it can operate at low temperatures and minimize secondary hazardous air pollutants in contrast to thermal incineration [2]. The recent advances in VOC catalytic oxidation have been reported in recent reviews [3–5]. Supported noble metals (Pt, Au, Pd) are commonly used in total oxidation of VOCs [6]. Although supported precious metal catalysts show excellent activities for the total oxidation of VOCs at low temperatures, the high cost of noble metals limits their wide applications. The key issue of such a technology is the availability of cheap, environmentally friendly and high-performance catalysts. In this way many trends have been carried out to comply with these criteria in the research of innocuous noble free catalysts as transition metal oxides. Generally metal oxide based catalysts are cheaper and more resistant to poisoning, but they are less durable and less efficient compared to supported noble-metal catalysts in the complete oxidation of VOCs [7]. Among them, bulk and supported manganese-based catalysts have received increased attention, as they are considered as cheap, environmentally friendly and active materials. Thus, it has been

* Corresponding authors.
E-mail addresses: jean-marc.giraudon@univ-lille1.fr (J.-M. Giraudon), jean-francois.lamonier@univ-lille1.fr (J.-F. Lamonier).

http://dx.doi.org/10.1016/j.apcatb.2017.06.072
0926-3373/

shown that manganese oxides such as Mn_3O_4, Mn_2O_3 and MnO_2 exhibited high activity for the complete oxidation of hydrocarbons [8].

Some studies have been performed on such catalysts, bulk [9–12] or supported [13–16], regarding more specifically the oxidation of toluene which is one of the major VOC released by industrial and automotive emissions and because it also possesses a high POCP (Photochemical Ozone Creativity Potential) [17,18]. In an attempt to get most promising catalyst formulations for toluene oxidation one effective strategy can be the investigation of binary metal oxides containing manganese. Among the different A-Mn-O systems, the Cu-MnO system has been found to be attractive since the mixture of manganese and cupric oxides have been led to the discovery of the general name "hopcalite" catalysts, of prime importance for CO oxidation at ambient temperature, O_3 destruction [19–22] and later for combustion of a wide range of VOCs at elevated temperatures [23–26]. Improved redox properties achieved by the formation of copper manganite $Cu_xMn_{3-x}O_4$ exhibiting flexible valences $Cu^{1+/2+}$ and $Mn^{3+/4+}$ and amorphous state stabilizing very small particles of copper and manganese oxides have been invoked to explain the good activity of hopcalite for CO oxidation. From these studies, Cu-Mn oxides can be viewed as promising catalysts but their performances closely depend on the method of preparation, all other things being equal. In order to improve the textural properties and intimate Cu-Mn interaction of copper-manganese oxides new synthesis routes have been developed in the literature that could replace the conventional ones such as co-precipitation [27,28] and solid state reaction [29]. The alternative routes include solgel [30], redox-precipitation [31,32], soft reactive grinding [33], synthesis under supercritical water conditions [34], reverse microemulsion [35], and the combustion method for formation of Cu–Mn oxide layers on the surface of Al metal foam [36]. Thus W.B. Li et al. [35] reported that reverse micro-emulsion method allows to get more efficient catalysts as compared to the co-precipitation route. In particular $Cu_{0.33}Mn_{0.67}O_x$ gives the highest activity for complete oxidation of toluene due to a better dispersion of the active phase [37].

In this work the effects of the preparation method of copper-manganese oxides and of noble metal (Pt; Pd) dopants were investigated in the complete oxidation of toluene and discussed in light of the physicochemical characterizations.

2. Experimental

2.1. Preparation of the catalysts

2.1.1. Preparation of $CuMn_2O_4$ by co-precipitation method

$CuMn_2O_4$ was prepared by hydrolysis of metal nitrates in aqueous solutions inspired by the work of Einaga et al. [37]. 30 mL of an aqueous solution of $Cu(NO_3)_2{\cdot}3H_2O$ (0.17 mol/L, Sigma-Aldrich, >99%) and $Mn(NO_3)_2{\cdot}4H_2O$ (0.33 mol/L, Sigma-Aldrich, >97%) were added dropwise to an aqueous solution of tetramethylammonium hydroxide (0.52 mol/L, Sigma-Aldrich, >97%). The suspension was equilibrated under stirring for 20 min at 25 °C. The resultant colloidal particles were filtered off and intensively washed with water followed by drying at 100 °C for 24 h. The powder was then calcined at 400 °C for 5 h to give a brown powder labelled $CuMn_2O_4$-P4 where P represents the (co-) precipitation method and i = 4 corresponds to the temperature of calcination of 400 °C. For comparison, Cu and Mn single oxides prepared in a similar way were labelled CuO_x-P4 and MnO_x-P4, respectively.

2.1.2. Preparation of CuMnOx by redox-precipitation method

The synthesis procedure was inspired from the one reported by Njagi et al. [31]. 100 mL of a solution of copper (II) nitrate ($Cu(NO_3)_2{\cdot}3H_2O$; 0.1 mol/L; Sigma-Aldrich, >99%) and of manganese (II) acetate solution ($Mn(CH_3COO)_2{\cdot}4H_2O$; 0.06 mol/L; Sigma-Aldrich, >99%) were added dropwise to an aqueous solution of $KMnO_4$ (50 mL, 0.12 mol/L) under constant stirring (350 rpm). The resulting suspension was stirred continuously for 24 h at 25 °C, filtered, washed and dried at 100 °C for 12 h to get a powder. The precursor was then calcined in dry air for 2 h at 200 °C or 300 °C (2 °C/min; 0.27 mL/(min.g)) to get a brown powder. The materials were labelled CuMnOx-Ri (i = 2; 3) where R stand for redox. For comparison, Mn single oxide was also prepared in a similar manner and labelled MnO_x-R3.

2.1.3. Preparation of M/CuMnOx (M = Pd, Pt)

The required amount of $Pd(NO_3)_2{\cdot}2H_2O$ (Sigma-Aldrich, >40%) or $Pt(NH_3)_4(NO_3)_2$ (Sigma-Aldrich, ≥50% Pt basis) was dissolved in 30 mL of distilled water to give the desired noble metal loading (0.5 wt%) before being added to the suitable amount of CuMnOx-R3 support. 440 mg of CuMnOx-R3 was added into the aqueous Pd(II) solution under constant stirring. The resulting mixture was stirred at 60 °C, in a rotary evaporator (20 rpm, 70 mbar), until the sample was dried and then kept for about 20 h in an oven at 80 °C overnight. The resulting materials were calcined at 300 °C for 4 h in air and were designated as M/CuMnOx-R3 (M = Pd, Pt).

A commercial Hopcalite catalyst named Purelyst MD101 was supplied by PureSphere Company and used as a reference. The granules were crushed into powder and used without any further pretreatment, the specific surface area was 290 m^2/g.

2.2. Catalyst characterization

Elemental analysis of Cu and Mn was performed on the calcined solids, using inductively coupled plasma – optical emission spectroscopy (ICP-OES) on an Agilent Technologies 700 Series spectrometer. Analysis was carried out at the REALCAT platform (University of Lille, Sciences and Technologies). Prior to analysis, the solids were treated by a mixture of concentrated hydrochloric and nitric acids (70%–30%).

The X-ray diffraction (XRD) patterns of the samples were recorded on a D8 Advanced Bruker AXS diffractometer using the Cu Kα X-ray radiation, 0.02° step size and 3 s step time over the 2 theta range: 10–70°. The crystalline phases were determined by the comparison of the registered patterns with the ICDD-JCPDS powder diffraction files processed on EVA software. Investigation of the evolution of the amorphous phase to crystalline(s) phases of CuMnOx-R3 with temperature in various atmospheres (air; N_2) was carried using a Bruker D8 advanced diffractometer (40 kV; 40 mA; CuK_α: 1.5418 Å) fitted with a XRK900 Environmental reaction chamber. The sample was placed on a glass ceramic (Macor) holder. The gas flow was 50 mL/min. The heating rate was 10 °C/min with diffraction patterns collected every 100 °C. Each data collection scan was between 10 and 70° (duration of a scan: 2h30 min). At a final temperature of 800 °C, the system was allowed to cool down to 25 °C.

The specific surface area of the catalysts was determined from N_2 adsorption at −196 °C from the single point method using the Micromeritics Flow Sorb III serial 416 apparatus. Before starting the analysis, the samples were degassed at 150 °C in nitrogen for 30 min.

When using a Micromeritics TriStar-II the adsorption-desorption experiments were performed after degassing for a few hours at 150 °C under vacuum. The BET surface (S_{BET}) and pore size distribution were calculated using the BET method and BJH method, respectively. The total pore volume (V_p) was estimated from the amount of nitrogen adsorbed at a relative pressure of 0.99.

The morphologies of catalysts were examined by Scanning Electron Microscopy images recorded on a Hitachi S-4700 apparatus. SEM micrographs at 10,000 × were taken with an accelerating voltage of 7 kV. Before SEM analysis, the samples were coated with Au via a JFC-1300 Auto Fine Coater (JEOL, Belgium) in order to avoid charge effects. After applying the gold coating, the catalysts powders were studied with an InTouch Scope JSM-6010 plus/LV Scanning Electron Microscope (SEM) (JEOL, Belgium).

The H_2 temperature-programmed reduction experiments were performed using a Micromeretics Autochem catalyst analyzer equipped with a quartz U-shaped micro reactor. The samples (0.050 g) were submitted to a 5% H_2/Ar gas mixture (50 mL/min) from 25 °C to 500 °C at a heating rate of 5 °C/min. The Mn average oxidation state (AOS) was determined from the hydrogen consumption considering the following hypotheses of Cu(II) into Cu(0) and of Mn^{x+} into Mn(II) reductions.

XPS spectra were recorded with a KRATOS, AXIS Ultra spectrometer with a Al Kα anode (1486.6 eV) and a hemispherical analyzer with constant ΔE/E. The binding energies (BE) were corrected using a value of 284.8 eV for the C 1s peak of the carbon species on the catalyst samples as an internal standard. Peak fitting was processed with CasaXPS. The fitting procedure allowed to determine the peak position, height and width.

The Mn AOS was determined by XPS from a relation based on a correlation between the binding energies of the doublet separation of Mn 3 s (ΔE) and the Mn AOS, proposed by Santos et al. [38]. The relation Mn AOS = 8.956–1.13 ΔE.

The XPS quantification of Cu and Mn was given by the Cu/Mn atomic ratio based on the intensities of Cu 2p and Mn 2p core levels. Due to overlapping of the Cu 2p and Mn LMM_b Auger peaks, the intensity of Cu 2p core level was extracted by removal of the contribution of the Mn Auger peak from the total envelope. Its relative contribution was estimated from the intensity (Mn 2p)/(Mn LMM_b) ratio of the MnOx-P4 oxide used as reference.

Positive and negative ToF-SIMS measurements were performed with a TOF·$SIMS_5$ spectrometer (ION-TOF GmbH Germany) equipped with a bismuth liquid metal ion gun (LMIG). The tableted samples were bombarded with pulsed Bi_3^+ primary ion beam (25 keV, 0.25 pA) rastered over a 500 × 500 μm^2 surface area. With a data acquisition of 100 s, the total fluence does not amount up to 10^{12} ions/cm^2 ensuring static conditions. Charge effects were compensated by means of a 20 eV pulsed electron flood gun. In these experiments, the mass resolution (m/Δm) was about 7000 at $m/z = 63$ for Cu^+. The secondary ions were identified by their exact mass, coupled with the appropriate intensities for the expected isotope pattern.

2.3. Catalytic tests

2.3.1. Light-off curves

Catalytic oxidation runs for abatement of toluene were performed in a continuous flow fixed bed Pyrex micro-reactor at atmospheric pressure. About 0.2 g of catalyst was placed in the reactor (1 cm in internal diameter) for each run. To obtain accurate and stable gas flow rates, mass flow controllers were used. The concentration of toluene was 800 ppmv, which was controlled by the temperature of a home-made saturator and the additional air stream. The flow rate of the gas mixture through the reactor was 100 mL/min, which gave a Gas Hourly Space Velocity (GHSV) of 30.000 mL/(g h).

The micro-reactor was placed in an electrical furnace providing the required temperature for catalytic reaction. Catalysts performances were evaluated by decreasing the temperature from 300 °C to 25 °C, with a decreasing rate of 0.5 °C/ min. Before each run, the samples were pretreated for 2 h at the temperature of calcination in flowing air (75 mL/min) for CuMn oxides and at 300 °C for the doped catalysts.

The concentrations of the inlet and outlet gas stream were analyzed online by Gas Chromatography (7860A Agilent Gas Chromatograph) equipped with a Thermal Conductivity Detector (TCD) and Flame Ionization Detector (FID) and with two columns: Restek Shin Carbon ST/Silco HP NOC 80/100 micropacked, to separate permanent gases (Air, CO and CO_2) and a capillary column Cp-Wax 52 CB25 m, Ø ¼ 0.25 mm, to separate hydrocarbons and aromatic compounds.

2.3.2. Reaction without oxygen in the feed

In order to assess the possible participation of catalyst oxygen in toluene oxidation, light-off curves were performed in oxygen free-atmosphere. Before each test, the samples were pretreated for 2 h at the temperature of calcination (300 or 400 °C) in air flow of 75 mL/min (5 °C/min). After cooling down to 25 °C, the catalyst was submitted to a gaseous toluene (800 ppmv)/He mixture (100 mL/min) until a steady state was achieved. At that stage catalyst performances were evaluated from 20 °C of 390 °C with a heating rate of 0.5 °C/min at a GHSV of 30.000 mL/(g h).

2.3.3. Tests of stability

Prior to the stability test, the catalyst was treated in air (75 mL/min) at the temperature of calcination for 2 h (10 °C/min). The catalyst was subsequently submitted with the same reactant mixture as mentioned above, at 150 °C, and the evolution of toluene conversion was monitored for 24 h.

Toluene conversion (C_t) was calculated as follows:

$$C_t\,(\%) = \frac{[CO_2]_{out}}{7[\text{toluene}]_{in}} \times 100$$

Where $[\text{toluene}]_{in}$ was the concentration introduced in the reactor and $[CO_2]_{out}$ was the CO_2 concentration in the off gas.

3. Results and discussion

3.1. ICP-OES results

The elemental composition of the various copper-manganese oxide catalysts is shown in Table 1. The Mn/Cu atomic ratio of 1.8

Table 1
ICP-OES analysis results.

	Mn/wt%	Cu/wt%	Mn/Cu[a]	K/wt%	Pd/wt%	Pt/wt%
MnOx-P4	74.43	–				
CuOx-P4	–	80.44				
$CuMn_2O_4$-P4	47.05	30.59	1.8			
MnOx-R3	54.97			4.04		
CuMnOx-R2	45.62	11.05	4.8			
CuMnOx-R3	48.41	11.66	4.8			
Pd/CuMnOx-R3	48.74	11.97	4.7		0.51	
Pt/CuMnOx-R3	46.96	11.26	4.8			0.40

[a] Atomic ratio.

Table 2
Textural and H_2-TPR properties of the catalysts.

	S_{BET} (m^2/g)	Vp[a] (cm^3/g)	H_2 ($mmol/g_{cata}$)	H_2/(Cu + Mn + M[b])	Mn AOS
MnOx-P4	27	0.14	5.85	0.43	2.9
CuOx-P4	8	0.05	12.83	1.01	–
$CuMn_2O_4$-P4	48	0.30	9.73	0.73	3.2
MnOx-R3	384	0.66	8.52	0.85	3.7
CuMnOx-R2	194	0.47	9.8	0.98	3.9
CuMnOx-R3	166	0.30	9.84	0.92	3.8
Pd/CuMnOx-R3	118	0.24	9.86	0.91	3.8
Pt/CuMnOx-R3	110	0.23	9.77	0.94	3.9

[a] BJH Desorption cumulative volume of pores.
[b] M = Pt or Pd.

is close to the expected value of 2.0 for $CuMn_2O_4$-P4 sample. Conversely a Mn/Cu atomic ratio of 4.8 for CuMnOx-Ri far exceeding the expected value of 1.0 indicates a copper loss. This result is in agreement with the work of Njagi et al. [31]. The partial copper loss resulting from the washing step of the preparation can be explained considering that Cu^{2+} ions were not directly involved in the redox reaction. It is also to be noted that small amount of K was detected on MnOx-R3 although intense washing.

3.2. Textural properties

Table 2 summarizes the textural properties of the different solids. The single oxides, namely CuOx-P4 and MnOx-P4, have BET surface areas of 8 and 27 m^2/g, respectively. Conversely the BET surface area of the Cu-Mn oxide of 48 m^2/g is significantly larger than those of the single oxides as previously observed [37]. The surface area of CuMnOx-Ri increases from 166 m^2/g up to 194 m^2/g with a decreasing calcination temperature of 100 °C. However these BET surface areas are less than that of MnOx-R3 oxide amounting to 391 m^2/g. The total pore volumes of the "redox-precipitation" samples which ranged from 0.30 to 0.66 cm^3/g are significantly higher than those of the co-precipitated samples ranging from 0.05 to 0.30 m^2/g. It is to be noted that the dispersion of Pt or Pd by wet impregnation on CuMnOx-R3 leads to decreased BET surface areas, most probably due to pore clogging. To sum up the redox-precipitation route allows to get improved textural properties for the catalysts as compared to the co-precipitation one.

3.3. X-ray diffraction patterns of the samples

The powder X-ray diffraction patterns of the Cu-Mn oxides prepared by the two methods are superposed in Figs. 1 and 2, respectively. The characteristic peaks of the spinel $CuMn_2O_4$ were observed for $CuMn_2O_4$-P4 (JCPDS 01-076-2296). Minor peaks due to traces of CuO were also detected. For the Cu single oxide (CuOx-P4), all peaks were indexed to the monoclinic CuO phase (JCPDS 016-0154) and no other peaks were detected. For MnOx-P4 sample, Mn_3O_4 (JCPDS 001-1127) along with Mn_5O_8 phase (JCPDS 007-1171), as a minor contribution, were observed. Conversely the MnOx and CuMnOx samples prepared from the redox-precipitation method have similar X-ray diffraction patterns showing two very broad diffraction peaks in the 33–40 and 63–70 2 theta regions implying they are essentially amorphous [31]. This apparently suggests the presence of (i) well dispersed/amorphous CuO_x or/and $Cu_xMn_yO_z$ phases imbedded in an amorphous MnO_x matrix and/or (ii) crystalline particles of above phases with average crystallite sizes or crystalline domains smaller than 2 nm. In order to get some additional information on the evolution of the amorphous phase to crystalline(s) phases with temperature and gas phase composition (air; N_2) the structural evolution of the CuMnOx-R3 sample has been investigated using in situ X-ray diffraction.

The resulting X-ray diffraction patterns have been plotted against temperature and presented in Figs. 3 and 4 considering air and N_2 treatment, respectively. As shown in Fig. 3 the material heated in air up to 400° C remained amorphous. X-ray diffraction

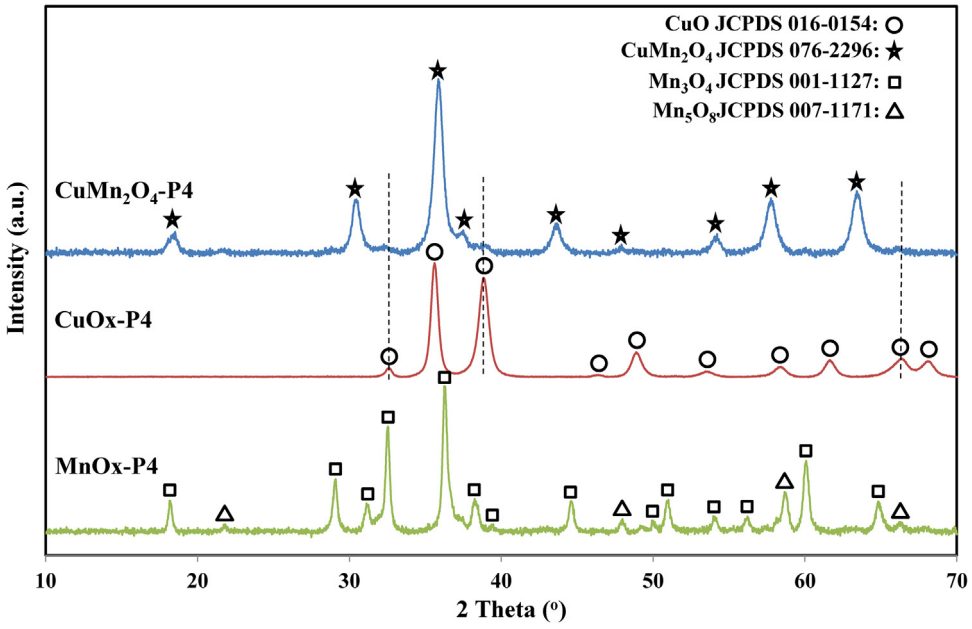

Fig 1. XRD patterns of co-precipitated samples.

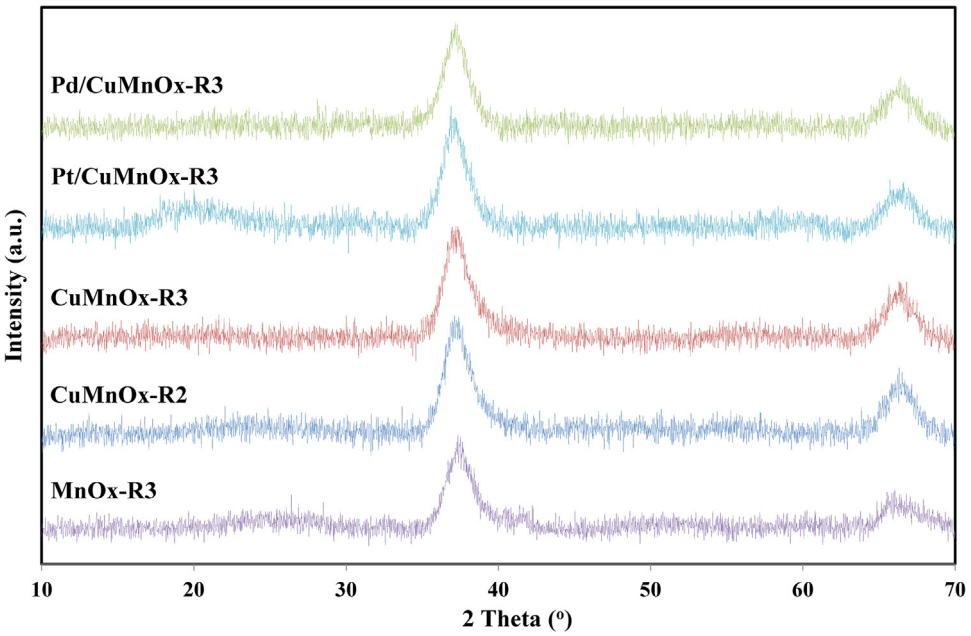

Fig. 2. XRD patterns of redox samples.

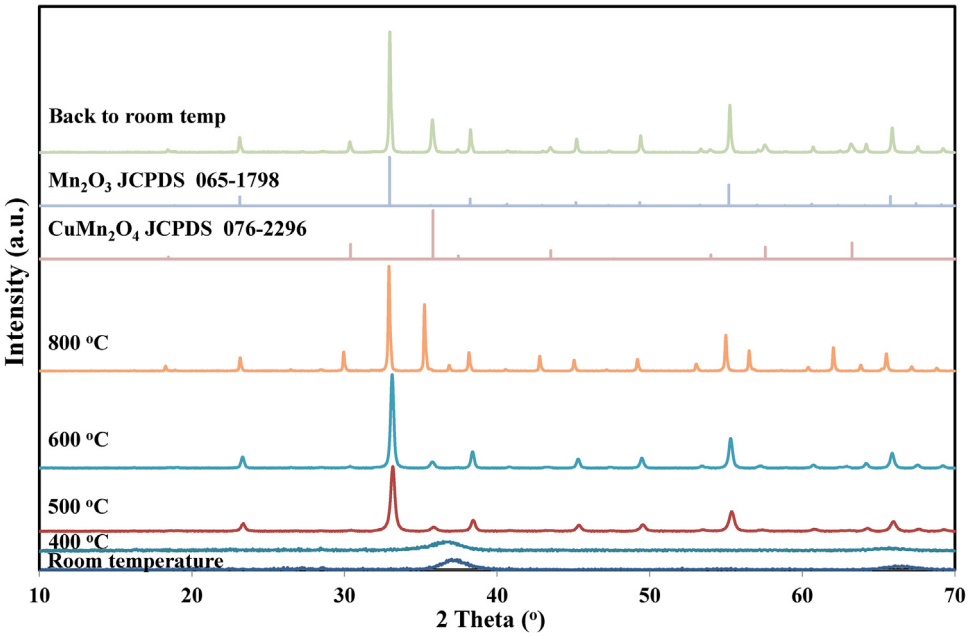

Fig. 3. In situ XRD patterns of CuMnOx-R3 under flowing air as a function of temperature.

patterns recorded from 500° C up to 800 °C revealed that Mn_2O_3 (JCPDS 065-1798) and $Cu_xMn_{3-x}O_4$ spinel oxide were formed and kept thermally stable in that temperature range. The thermal stability of the amorphous phase is also effective up to 400 °C when heating in N_2 (Fig. 4). At 500 °C the transformation of the amorphous phase takes place into Mn_3O_4 as predominant phase and related spinel $Cu_xMn_{3-x}O_4$ as the minor one. Upon heating at 600 °C the X-ray diffraction pattern reveals the presence of additional $CuMnO_2$ oxide (crednerite) at the expense of the $Cu_xMn_{3-x}O_4$ phase. Such a phase has been already observed resulting from the decomposition of $CuMn_2O_4$ when heated at 350 °C involving the removal of lattice oxygen according to the formal reaction [39]:

$$CuMn_2O_4 = 3CuMnO_2 + Mn_3O_4 + O_2$$

Back to room temperature does not change the distribution of the related oxide phases.

3.4. SEM characterization

The SEM image in Fig. S1 clearly displays that CuO particles in CuOx-P4 have an ellipsoidal shape with an average length of 1000 nm and a width of 200 nm. The SEM picture of MnOx-P4 clearly shows randomly distributed spherical grains with small size of 100 nm diameter along with agglomerates. The surface morphology of $CuMn_2O_4$-P4 also shows quasi-spherical grains along with higher agglomerated grain structures as in MnOx-P4 sample. In comparison the SEM image of CuMnOx-R3 shows particles of near

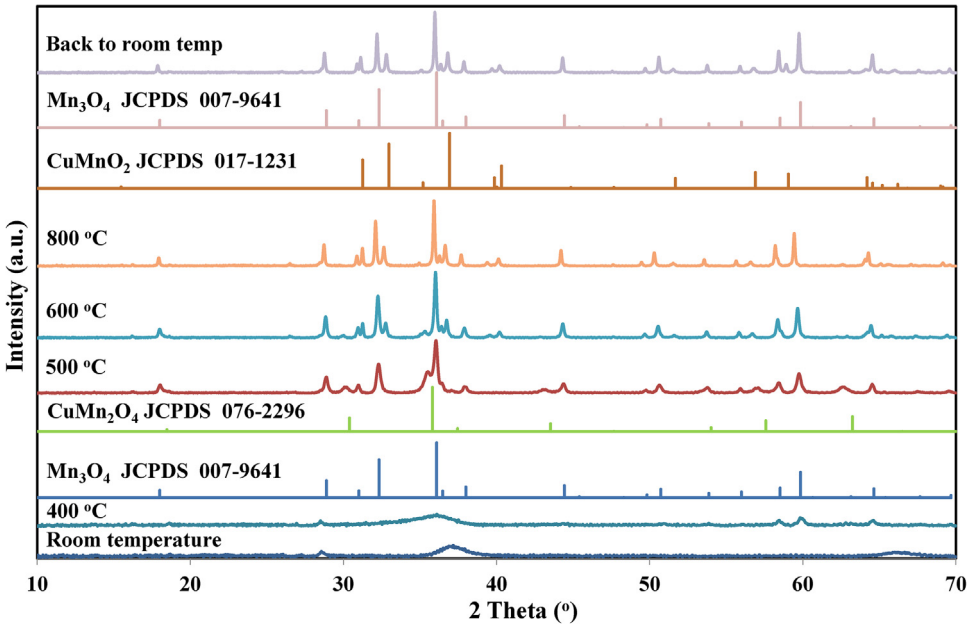

Fig. 4. In situ XRD patterns of CuMnOx-R3 under flowing N_2 as a function of temperature.

spherical morphology with homogeneous size distribution which characteristics are retained in the doped catalysts.

3.5. H_2-TPR studies

H_2 temperature-programmed reduction profiles of related CuMn mixed oxides are shown in Fig. 5a and b and the resulting H_2 consumption as well as the Mn AOS are given in Table 2. The TCD trace relative to $CuMn_2O_4$-P4 showed one asymmetric peak (150–320 °C) in accordance with the results of Einaga et al. [37]. This suggests that the copper and manganese cations are reduced practically at the same temperature in the spinel lattice. Additionally the low temperature H_2 consumption may possibly arises from the reduction of small crystallites of CuO/MnOx well dispersed on the oxide matrix. We determined a Mn AOS of 3.1 in CuMnOx-P4 based on the corrected H_2 consumption taking into account the reduction of Cu(II) into Cu(0). This is in agreement with the Mn AOS of 3.2 given by H. Einaga et al. using a linear relationship between the Mn AOS and absorption edge obtained from the Mn K-edge XANES spectra [37]. The CuOx-P4 sample shows only a peak of H_2 consumption in the range 140–300 °C indicating its high oxidizing ability. MnOx-P4 shows two reduction regions in the temperature range 160–320 °C and 320 °C–450 °C. The first one refers to the reduction of Mn_5O_8 to Mn_3O_4 and the second one to the reduction of Mn_3O_4 to MnO [40] in line with the X-ray diffraction results. The non-observance of the peak at high temperature for $CuMn_2O_4$-P4 has been previously explained by the role of Cu(0) promoting the reduction of manganese oxide by H_2 [37].

The TCD traces relative to $CuMnO_x$-Ri (i = 2,3) samples in Fig. 5b are rather similar showing a broad asymmetric peak in the temper-

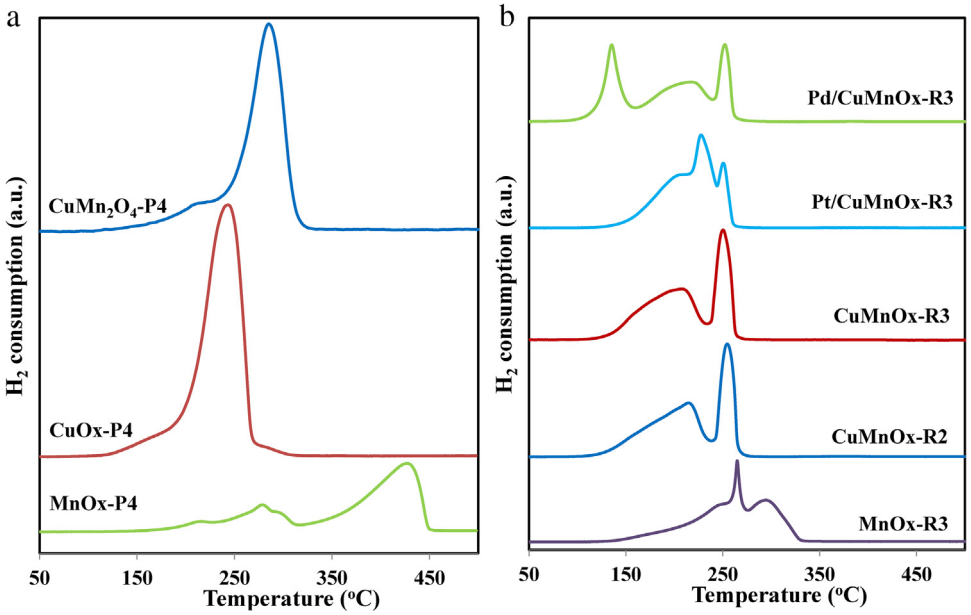

Fig. 5. H_2-TPR profiles of the fresh catalysts prepared: (a) from co-precipitated method; (b) from redox-precipitation method.

Table 3
XPS results on the fresh samples.

Sample	Cu $2p_{3/2}$ BE (eV)	Mn $2p_{3/2}$ BE (eV)	Mn/Cu[a]	AOS Mn	O_1 BE (eV)	O_2 BE (eV)	O_3 BE (eV)	O_1 (at%)	O_2 (at%)	O_3 (at%)	O_2/O_1
MnOx-P4	–	641.7	–	3.0	529.7	531.5	533.4	61.3	28.3	10.4	0.46
CuOx-P4	933.3	–	–	–	529.6	531.3	533.5	55.6	38.6	5.8	0.69
$CuMn_2O_4$-P4	931.2, 934.0	642.0	3.7	3.7	529.8	531.6	533.7	43.8	39.3	8.3	0.90
MnOx-R3		642.4	–	3.4	529.8	531.5	533.8	58.1	38.1	3.8	0.66
CuMnOx-R2	934.3	642.2	5.0	3.3	530.0	531.2	533.7	51.7	43.3	5.0	0.84
CuMnOx-R3	934.3	642.4	5.1	3.5	530.0	531.3	533.8	52.1	43.9	4.0	0.84
Pd/CuMnOx-R3	934.0	642.0	5.1	3.4	529.8	531.5	533.5	47.7	39.3	13.0	0.82
Pt/CuMnOx-R3	934.0	642.2	5.1	3.4	529.8	531.5	533.6	48.5	43.9	7.6	0.90

[a] Atomic ratio.

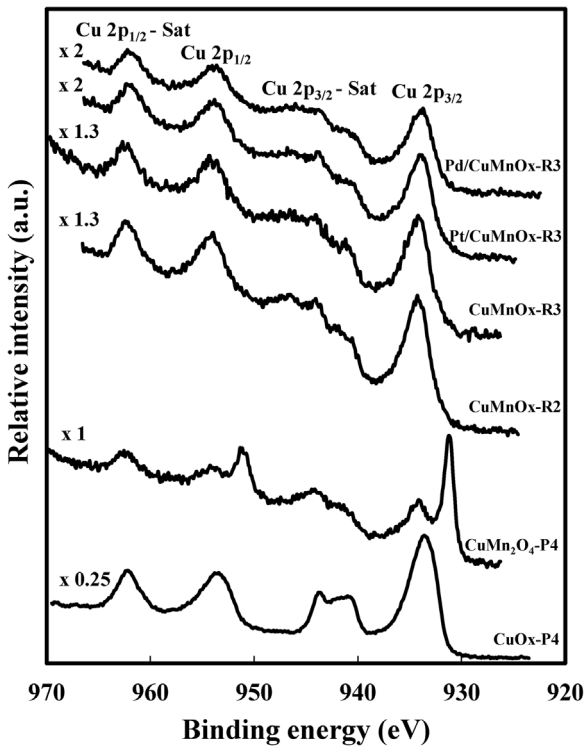

Fig. 6. XPS Cu 2p core level recorded on the fresh catalysts.

ature range 120–240 °C at 210 °C ± 5 °C followed by a symmetric narrow peak at about 250 ± 5 °C. These curves differ from that of MnOx-R3 which exhibits two broad peaks at 244 and 295 °C along with a narrow peak in between at 265 °C. The Mn AOS of 3.7 for MnOx-R3 increases up to 3.8 and 3.9 for the CuMnOx materials calcined at 200 and 300 °C, respectively. These findings are consistent with a Mn AOS of 3.8, using potentiometric titration method, performed on a MnO_x catalyst prepared in a similar manner by Njagi et al. but without calcination by the redox-precipitation method [31]. Consequently a mixed valent environment with Mn^{4+} being predominant can be invoked in this catalyst series. Pd and Pt dispersed on CuMnOx-R3 affect the H_2-TPR profiles while the total amount of consumed H_2 keeps rather constant. The TPR-profile of Pd/CuMnOx-R3 reveals a new peak at 135 °C while the remaining shape of the curve resembles that of CuMnOx-R3. The amount of hydrogen consumed in the low temperature peak can be consistent with the total reduction of PdO into metallic Pd promoting the reduction of Cu^{2+} and Mn^{n+} cations at the vicinity of the metallic palladium interface by hydrogen spill-over process. By opposition the H_2-TPR trace of Pt/CuMnOx shows three overlapping peaks at 204, 230 and 251 °C. The non-observance of a low H_2 consumption can be due here to higher temperature of platinum reduction as compared to palladium. It is to be noted that the Mn AOS keeps at 3.8–3.9 for the doped catalysts shows no significant changes of the state of manganese.

3.6. XPS analysis

XPS data recordings given in Table 3 were used to investigate the oxidation states of copper and manganese in the different catalysts. The Cu $2p_{3/2}$ envelope shows two distinct peaks for the spinel $CuMn_2O_4$-P4 (Fig. 6). The signal at 931.1 eV is due to monovalent copper Cu^+ in accord with previously reported data [41]. The signal of lower intensity at 934.1 eV together with its satellite between 938 and 948 eV is indicative of divalent copper Cu^{2+} [42–44]. Integration of the signals leads to a Cu^+/Cu^{2+} ratio close to

Table 4
List of the $Cu_xMn_yO_zH_w$ ions in polarity (+) and (−).

$Cu_xMn_yO_zH_w^+$	$CuMn_2O_4$-P4 intensity ($/10^3$ count/s)	CuMnOx-R3 intensity ($/10^3$ count/s)	$Cu_xMn_yO_zH_w^-$	$CuMn_2O_4$-P4 intensity ($/10^3$ count/s)	CuMnOx-R3 intensity ($/10^3$ count/s)
MnCuO	73.82	59.89	$CuMn_2O_4$	3.39	2.00
^{65}CuMnO	34.31	29.07	$CuMn_2O_4H^-$	0.87	1.15
CuMnOH	7.24	11.09	$^{65}CuMn_2O_4$	2.29	1.48
^{65}CuMnOH	3.58	5.13	$CuMn_2O_5$	3.99	1.94
CuMn	15.99	18.62	$CuMn_2O_5H^-$	0.96	1.27
CuMnH	7.97	2.86	$^{65}CuMn_2O_5$	2.17	1.40
$CuMnO_2$	4.00	3.85	$CuMn_3O_5$	3.34	2.30
$CuMnO_2H^+$	6.27	12.87	$CuMn_3O_5H^-$	0.57	0.85
$CuMnO_2H_2$	5.90	13.38	$^{65}Cu\ Mn_3O_5$	1.51	1.02
$^{65}CuMnO_2H$	3.57	6.29	$CuMn_3O_6$	3.84	2.06
$^{65}CuMn\ O_2H_2$	2.51	5.33	$CuMn_3O_6H^-$	0.61	0.70
$CuMn_2O_2$	21.40	13.86	$^{65}Cu\ Mn_3O_6$	1.97	1.12
$^{65}Cu\ Mn_2O_2$	16.97	7.37	$CuMn_4O_6$	1.01	0.82
$CuMn_2O_3$	8.36	5.58	$CuMn_4O_6H^-$	0.31	0.57
$^{65}CuMn_2O_3$	4.95	5.82	$CuMn_4O_7$	1.29	0.73
$CuMn_2O_3H$	4.57	8.45	$CuMn_4O_7H^-$	0.28	0.40
$^{65}CuMn_2O_3H$	2.44	3.73	$^{65}Cu\ Mn_4O_7$	0.83	0.40
$CuMn_3O_3$	8.43	8.29			
$^{65}CuMn_3O_3$	5.21	4.03			
$CuMn_3O_4$	7.22	5.32			
$^{65}CuMn_3O_4$	3.90	3.25			
$CuMn_4O_5$	4.15	3.18			
$^{65}CuMn_4O_5$	2.67	1.84			
$CuMn_4O_4$	3.68	4.14			
$^{65}CuMn_4O_4$	2.60	1.97			
$CuMn_5O_5$	1.58	2.20			
$^{65}CuMn_5O_5$	1.02	1.02			
$CuMn_5O_6$	2.20	1.90			
$^{65}CuMn_5O_6$	1.46	1.10			
Sum	267.97	251.46	Sum	29.23	20.21
$Cu_xMn_yO_zH_w^+$ (%)	9.06	5.99	$Cu_xMn_yO_zH_w^-$ (%)	2.80	2.85

0.5. The formation of Cu^+ takes place owing to the redox equilibrium $Cu^{2+} + Mn^{3+} = Cu^+ + Mn^{4+}$ [41] without excluding some partial reduction of Cu^{2+} under the X-ray beam. This is supported by the XPS Mn AOS of 3.7 which agrees with a mixture of $Mn^{4+/3+}$ with Mn^{4+} as the predominant cation. Additionally the atomic Mn/Cu ratio of 3.7 shows an excess of Mn at the catalyst surface. Conversely the CuMnOx-Ri oxides exhibit one single Cu $2p_{3/2}$ photopeak with BE of 934.2 (±0.2 eV) ascribed to the presence of Cu^{2+} (Fig. 6). The XPS Mn AOS of 3.3 ± 0.2 eV is in accordance with Mn^{3+} as dominant oxidation state on contrary to H_2-TPR results. The XPS atomic Mn/Cu ratio of 5.1 agrees with that of elemental analysis of 4.8 attesting of a good dispersion of the Cu-Mn oxide particles. The state and dispersion of the metal dopants (Pd; Pt) dispersed on CuMnOx-R3 have also been investigated. The Pd 3d core level doublet (not shown here) has well separate spin-orbit components Pd $3d_{3/2}$ and Pd $3d_{5/2}$ separated by 5.3 eV. The Pd $3d_{5/2}$ component at about 337.4 eV has been attributed to Pd in a high oxidation state (+3/+4) existing at the catalyst surface [45]. The Pd/(Mn + Cu) ratio of 0.018 as compared to the value of 0.0044 from elemental analysis shows a surface enrichment of Pd. Regarding Pt/CuMnOx-R3, as the Pt 4f core level is drawn in the Cu 3p envelope, the presence of Pt is only detected by the observance of Pt $4d_{3/2}$ core-level of low intensity precluding quantification and determination of the accurate oxidation state of Pt in the sample. The O1s spectra for all samples were fitted using three contributions. The O_1 component with BE ranging from 529.6 to 530.0 eV was characteristic of lattice oxygen (O^{2-}) [12]. The O_2 component with BE of 531.3–531.5 eV was ascribed to surface oxygen ions with low coordination [12] while O_3 contribution was related to adsorbed water on the surface. It is to be noted that the formation of oxygen adspecies due to the presence of surface oxygen vacancies is generally believe to be an important parameter to consider in the catalytic activity. The values of the intensity O_2/O_1 ratios listed in Table 3 have been used to quantify such species. It is found the highest values for the redox based catalysts, the $CuMn_2O_4$-P4 and Pt/CuMnOx-R oxides exhibiting the highest value of 0.9 in each series.

3.7. ToF-SIMS analysis

Time-of-flight secondary ion mass spectrometry (ToF-SIMS) analyses have been performed in static conditions on fresh $CuMn_2O_4$-P4 and CuMnOx-R3 catalysts in order to get molecular information about the surface as ToF-SIMS enables to probe the top layers (1–3 nm) of the catalysts. It is to be noted the detection of $Cu_xMn_yO_zH_w$ secondary ions both in polarities (+) and (−) which have been compiled in Table 4. As an example the $CuOMn^+$ secondary signal has been reported for the two Cu-Mn oxides in Fig. 7. Such family of ions contributes in relative intensity to 9.0% and 6.0% in polarity (+) and to 2.80% and 2.85% in polarity (−) based on the total intensity of significant secondary ions for $CuMn_2O_4$-P4 and CuMnOx-R3, respectively. The detection of such secondary ions in significant amount is indicative of an intimate intermixing of Mn, Cu and O leading to compositionally homogeneous nanoscale materials.

3.8. Light-off curves

The conversion of toluene into CO_2 as a function of catalyst temperature is plotted in Fig. 8. T_{10}, T_{50} and T_{90}, the temperatures at which respectively 10%, 50% and 90% of toluene is converted into CO_2 as well as the specific and intrinsic rates at 170 °C are listed in Table 5. Adding copper to manganese by co-precipitation improves the toluene conversion (Fig. 8a). Indeed the activity of the catalysts based on T_{50} value (in °C) decreases as follows: $CuMn_2O_4$-P4 (195) > MnO_x-P4 (207) > CuO_x-P4 (228). This order is maintained when considering T_{10} and T_{90}. Comparatively the redox-precipitation based catalysts are more active with a T_{50} value of 173 °C for the most active CuMnOx-R2 catalyst which

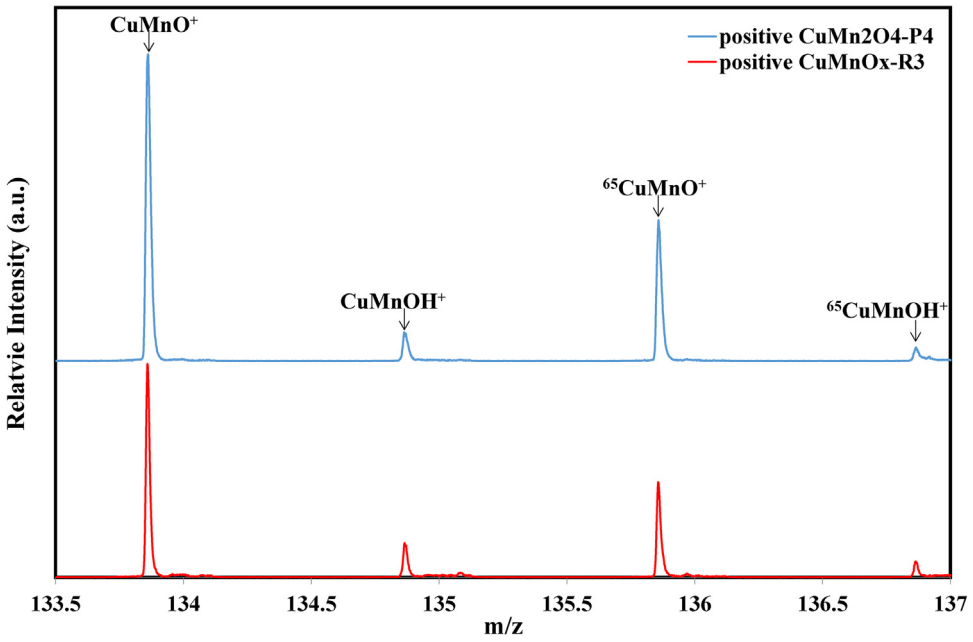

Fig. 7. ToF-SIMS spectra in polarity (+); *m*/*z* range: 133.5-137.

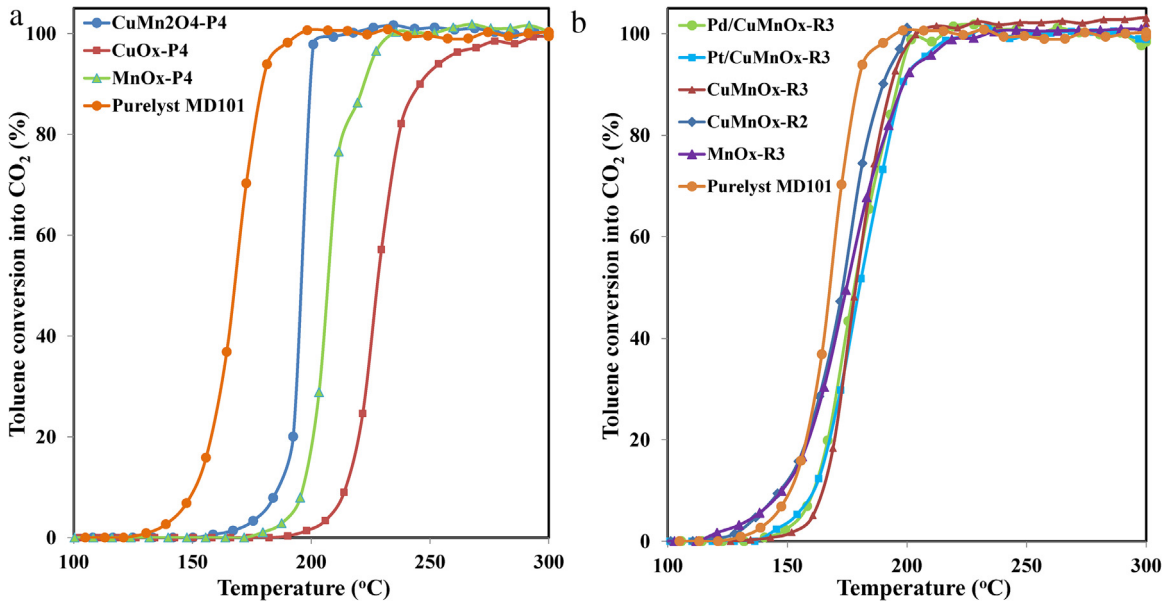

Fig. 8. Light-off curves of the fresh catalysts prepared: (a) from co-precipitated method; (b) from redox-precipitation method – Comparison with commercial Purelyst MD101 sample.

Table 5
Catalytic results based on toluene conversion into CO_2.

Catalyst sample	GHSV (h^{-1})	T_{10} (°C)	T_{50} (°C)	T_{90} (°C)	r^a (μmol/h g)	r^a (μmol/h m^2)	C_t[c] (%)	r_1[b] (μmol/h g)	r_1[b] (μmol/h m^2)
MnOx-P4	21700	196	207	223	–	–	–	–	–
CuOx-P4	29700	215	228	247	–	–	–	–	–
$CuMn_2O_4$-P4	27800	185	195	200	22	0.45	0.14	1.9	0.04
MnOx-R3	16500	147	174	199	401	1.04	–	–	–
CuMnOx-R2	6100	146	173	190	420	2.17	4.41	43	0.22
CuMnOx-R3	8200	164	179	194	205	1.23	2.09	20	0.12
Pd/CuMnOx-R3	7700	160	178	196	289	2.45	2.11	21	0.18
Pt/CuMnOx-R3	8900	160	180	198	251	2.28	2.27	22	0.20
Purelyst MD-101	13200	151	168	180	550	1.90	3.88	38	0.13

Toluene (800 ppmv)/air.
[a] Reaction rate at 170 °C (light-off curves).
[b] Reaction rate at 150 °C (stability test).
[c] Estimated at the end of stability test.

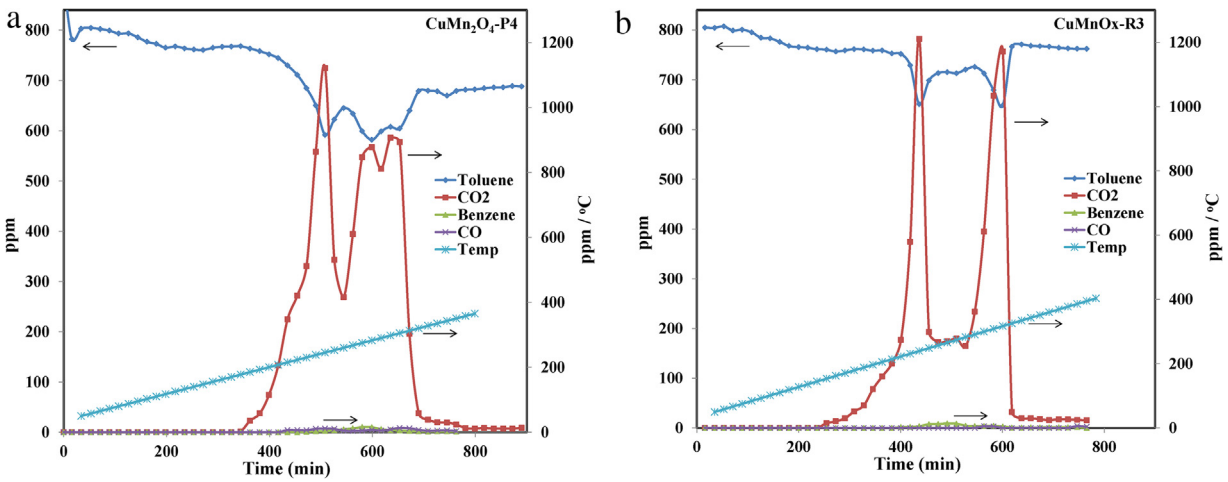

Fig. 9. Evolution of the gaseous species as a function of temperature in toluene oxidation performed in helium in the presence of (a) co-precipitated and (b) redox catalyst.

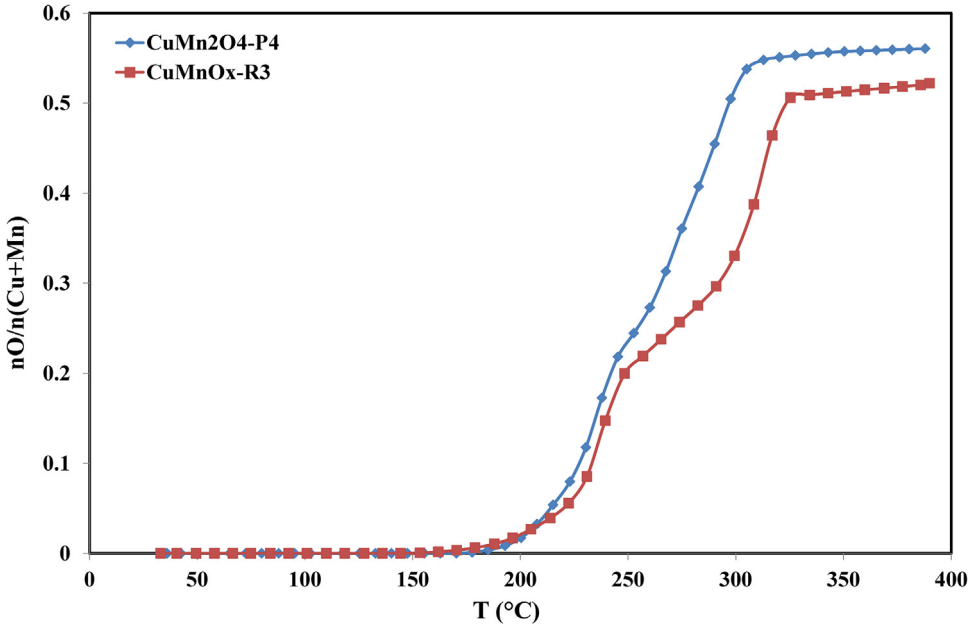

Fig. 10. Evolution of the atomic O/(Mn + Cu) as a function of temperature in toluene oxidation performed in helium.

compares well with that of Purelyst MD101 catalyst at 170 °C. Although the MnOx-R3 and CuMnOx-Ri catalysts have a similar T_{50}, at about 175 °C, the mixed oxides appear more active at higher temperature as attested by the T_{90} values. The intrinsic rate (in μmol/(h m^2)) at 170 °C decreased in the following order: CuMnOx-R2 (2.17) > CuMnOx-R3 (1.23) > MnOx-R3 (1.04) as shown in Table 5. The higher intrinsic rate of CuMnOx-R2 than that of CuMnOx-R3 was ascribed to an improvement of textural properties induced by a decrease of calcination temperature. Hence the good toluene conversion on CuMnOx-R2 was ascribed to the high surface density of catalytic sites in correlation with its high specific surface area and to an improvement of the active site quality.

Adding Pt or Pd to CuMnOx-R3 does not improve the toluene conversion (Fig. 8b). The comparison of the performances of Pt/CuMnOx-R3 or Pd/CuMnOx-R3 catalysts with alumina supported Pt or Pd ones studied in literature is performed through an overview Table containing for each study the nature of the support, the noble metal weight percentage, the toluene concentration, the gas hourly space velocity and the T_{50} (Table S1). Based on this literature review, the works of Liotta et al. [46] (Pt/γ-Al_2O_3) and Kim et al. [47] (Pd/γ-Al_2O_3) can be selected for comparison since the experimental test conditions used in both studies are similar to those we have employed. Despite low noble metal loading (0.5 wt%), the catalytic performances of PtCuMnOx-R3 and PdCuMnOx-R3 can be favorably compared with those of Pt(1 wt%)/γ-Al_2O_3 (T_{50} = 180 °C) [46] and Pd((1 wt%)/γ-Al_2O_3 T_{50} = 220 °C) [47], respectively (Table S1).

It is to be noted that benzene and benzaldehyde are detected as trace amounts in the course of the catalytic reaction.

3.9. Reaction without oxygen in the feed

Reactions without oxygen in the feed were also performed over $CuMn_2O_4$-P4 and CuMnOx-R3 catalysts in order to assess the possible participation of catalyst oxygen in toluene oxidation. The evolution of the concentrations of toluene, CO_2, CO and benzene were recorded as a function of temperature in Fig. 9. Whatever the catalyst under concern the toluene consumption occurred in two steps: one at low temperature with a maximum toluene consumption at about 240–245 °C and a second one step at

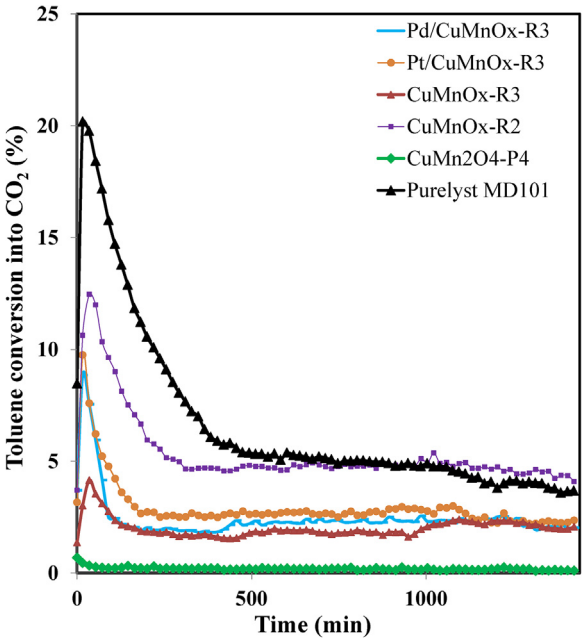

Fig. 11. Stability tests on the different catalysts at 150 °C.

higher temperature characterized by 2 maxima at 283 and 298 °C for $CuMn_2O_4$-P4 (Fig. 9a) while only a maximum at 317 °C was detected for CuMnOx-R3 (Fig. 9b) catalyst. The CO_2/Toluene molar ratio of 6.6 ($CuMn_2O_4$-P4) and 6.8 (CuMnOx-R3) was in accordance with that expected of 7.0, considering the margin of error, in line with a negligible production of CO in the course of the reaction. Hence, the oxidation of toluene occurs in the absence of any gaseous oxygen. The presence of two consecutive peaks separated by about 40 °C ($CuMn_2O_4$-P4) and 80 °C (CuMnOx-R3) can be explained by the successive participation of surface (sub-surface lattice oxygen) and lattice oxygen in copper-manganese oxides. The amount of oxygen extracted from the solids respective to the metal content O/(Cu + Mn) as a function of temperature was given

Table 6
Textural and H_2-TPR properties of the catalysts after stability test.

	S_{BET} (m^2/g)	Vp[a] (cm^3/g)	H_2 (mmol/g)
UCuMnOx-R3	189	0.45	5.26
$UCuMn_2O_4$-P4	30	0.30	8.95
UPd/CuMnOx-R3	167	0.42	6.92
UPt/CuMnOx-R3	188	0.50	6.19

[a] BJH Desorption cumulative volume of pores.

in Fig. 10. It is found a similar O/(Cu + Mn) trace with temperature regarding the first step to reach a value of 0.22 while in the second step the O/(Cu + Mn) trace was translated to higher temperatures on CuMnOx-R3 to reach a final value at 390 °C of 0.53 and 0.56 for CuMnOx-R3 and $CuMn_2O_4$-P4, respectively. It was shown that transformation of the $CuMn_2O_4$-P4 catalyst readily occurred to give MnO and Cu^0 (XRD analysis). By opposition the XRD characteristic peaks of $Cu_{0.1}Mn_{2.9}O_4$ and $Cu_{1.5}Mn_{1.5}O_4$ phases were found for CuMnOx-R3 catalyst.

3.10. Test of stability

24 h stability tests have been performed at 150 °C on all undoped and doped copper-manganese oxides and the toluene conversion into CO_2 as a function of time is given in Fig. 11. The Purelyst MD101 catalyst strongly deactivates in the six first hours and after smoothly linearly deactivates over time. In comparison a partial deactivation at the early stages of the reaction occurs on CuMnOx-Ri and M/CuMnOx-R3 (M=Pt, Pd) before achievement of a quasi-stationary state. At the final stage of the reaction no improvement is observed with the doped catalysts as compared to the CuMnOx-R3 active support. Conversely the low calcining temperature is beneficial as CuMnOx-R2 has the higher specific activity of 43 μmol/(g.h) towards all catalysts even the Purelyst MD101 (38 μmol/(g.h)). Additionally this beneficial effect is amplified when considering the intrinsic rates which is 1.7 times higher than that of Purelyst MD101.The $CuMn_2O_4$-P4 catalyst for its part seems to be quite stable over time but its activity keeps very low. The physico-chemical characterizations of the used catalysts are displayed in Table 6. The X-ray diffraction patterns (not shown

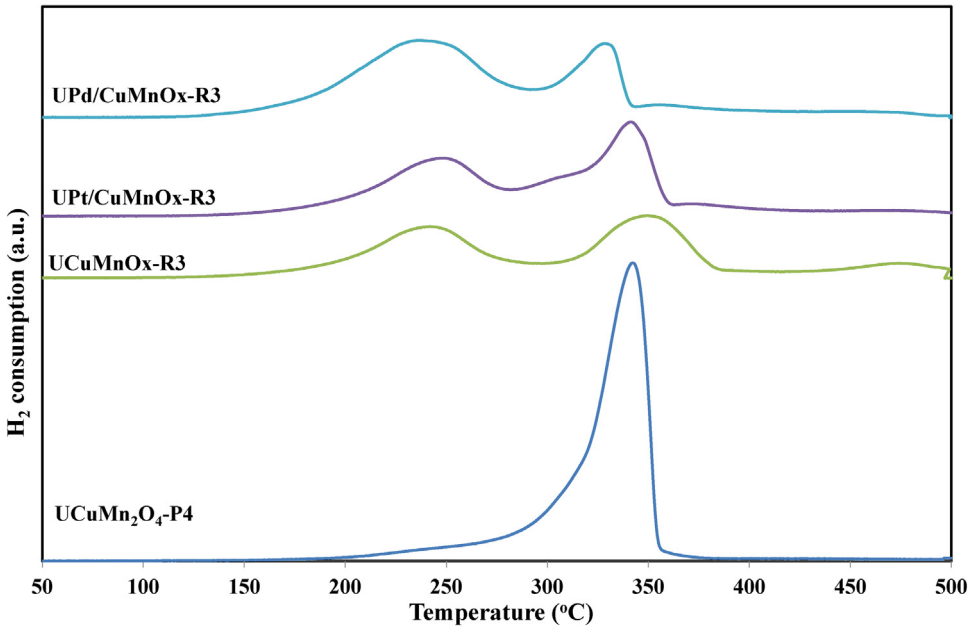

Fig. 12. H_2-TPR profiles of the UCuMnOx based catalysts (U stand for used catalyst).

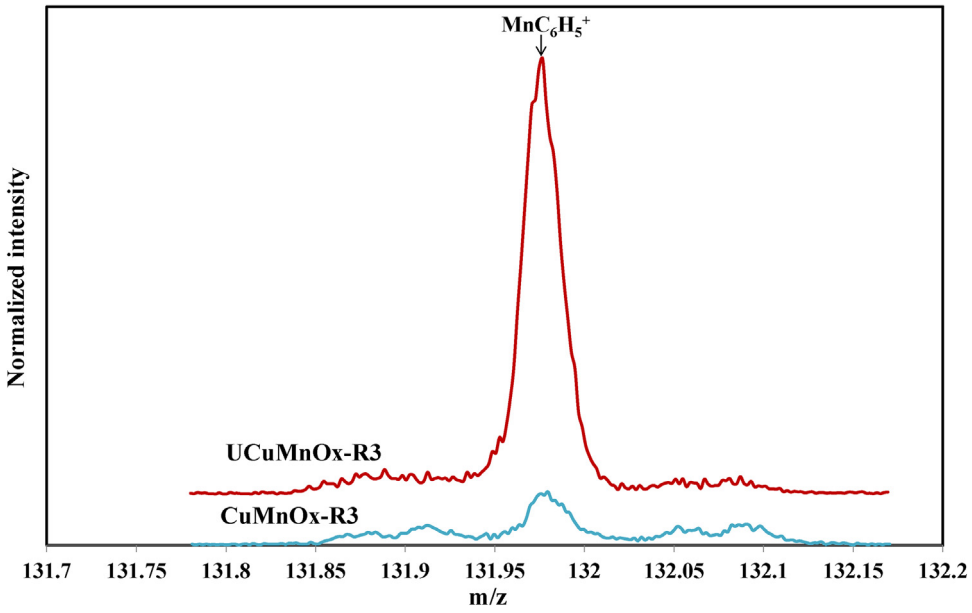

Fig. 13. Positive ToF-SIMS spectra of CuMnOx-R3 and UCuMnOx-R3 in the *m*/*z* range: 131.8–132.15. (U stand for used catalyst).

here) do not change significantly over the course of the reaction. While the BET surface area reduces by one third for $CuMn_2O_4$-P4 those of the "redox-precipitation" series keep stable and even slightly increase. By opposition the H_2-TPR profiles of the used catalysts given in Fig. 12 as well as the amount of H_2 consumed are significantly affected as compared to those of the fresh catalysts. For CuMnOx-R3 it is found now two broad H_2 consumptions in a larger temperature range 140–380 °C to be compared to that of 110 °C–260 °C on the fresh catalyst. It is also to be noted that the amount of H_2 consumption decreases by a factor 2. This clearly indicates a partial reduction of Cu^{2+} and/or Mn^{n+} species due to toluene acting as a reductant in agreement with the previous experiments without oxygen. Similar trends are observed in terms of temperature range and amount of consumed hydrogen when considering the noble metal doped catalysts. In comparison the H_2-TPR profile of $UCuMn_2O_4$-P4 (used $CuMn_2O_4$-P4) is rather similar but shifted to higher temperature with a H_2 consumption slightly affected.

ToF-SIMS mass spectra obtained in polarity (+) and (−) of UCuMnOx-R3 (used CuMnOx-R3) showed new secondary peaks compared to that of the fresh catalyst. These secondary ions were found to be derived from toluene (m/z = 77.04; $C_6H_5^+$) and to some organic intermediates of the reactions such as benzene (m/z = 77.04; $C_6H_5^+$), phenol (m/z = 93.03; $C_6H_5O^-$), benzaldehyde (m/z = 105.03; $C_7H_5O^+$) and benzoic acid (m/z = 121.03; $C_7H_5O_2^-$). Additionally ToF-SIMS allows to see some metal-organic secondary ions. The detection of such ions gave direct information related to adsorbed organic species on the metal oxide surface. The m/z value at 131.97 identified as $MnC_6H_5^+$ is ascribed to adsorbed benzene on Mn related site (Fig. 13). Quite similarly it is worth to mention the detection of $CuC_6H_4^+$ at m/z = 139.95 but with a relative lower intensity. The m/z value at 163.97 is likely attributed to adsorbed benzaldehyde on Mn ($MnC_6H_5O_2^-$). Hence ToF-SIMS allows to observe fragment ions relative to adsorbed products resulting from the partial oxidation of toluene. It can be proposed that the presence of adsorbed organic species at the surface could also account for the deactivation. This deactivation is less pronounced on CuMnOx-R2 allowing to preserve an activity with time on stream at 150 °C.

4. Conclusion

At least, four relevant conclusions can be drawn from this study:

(i) Whatever the method of synthesis, the CuMnOx catalysts outperformed the reference single oxides in total toluene oxidation. Moreover the CuMnOx-R2 catalyst outclassed the Purelyst MD101 commercial catalyst over time on stream.
(ii) The dispersed copper manganese oxides using the redox-precipitation route exhibit much higher activity as compared to that of the spinel $CuMn_2O_4$-P4 oxide prepared by co-precipitation using TMAH as precipitant. The superior performance of the redox derived Cu-Mn materials was attributed to improved textural properties such as high surface areas, amorphous state and structural disorder (presence of oxygen vacancies).
(iii) From catalytic experiments performed in free oxygen atmosphere it is deduced that surface adsorbed (O_{ads}) oxygen and subsurface oxygen play a role in the activity of the catalyst.
(iv) The ToF-SIMS analysis after test allows to detect metal (M = Mn, Cu) organic secondary ions attesting of strong adsorption of partial oxidation/decomposition products of toluene on active sites inducing partial deactivation.

Acknowledgements

The joint research program PICS n°6913 (Preparation of catalysts and catalytic depollution assisted by plasma) from CNRS, the "DepollutAir" project of the European Program INTERREG V France – Wallonie – Flanders (FEDER), Chevreul institute (FR 2638), Ministère de l'Enseignement Supérieur et de la Recherche and Région Hauts-de-France are acknowledged for supporting and funding this work. The authors are grateful in particular to Olivier Gardoll (Lille1 University, France) for the TPR analyses, Martine Trentesaux for XPS analysis and Laurence Burylo for XRD measurements.

Appendix A. Supplementary data

Supplementary data associated with this article can be found, in the online version, at http://dx.doi.org/10.1016/j.apcatb.2017.06.072.

References

[1] K. Tzortzatou, E. Grigoropoulou, Catalytic oxidation of industrial organic solvent vapors, J. Environ. Sci. Health. Part A 45 (2010) 534–541.
[2] J.J. Spivey, Complete catalytic oxidation of volatile organics, Ind. Eng. Chem. Res. 26 (1987) 2165–2180.
[3] Z. Zhang, Z. Jiang, W. Shangguan, Low-temperature catalysis for VOCs removal in technology and application: a state-of-the-art review, Catal. Today 264 (2016) 270–278.
[4] M. Tomatis, H.-H. Xu, J. He, X.-D. Zhang, Recent development of catalysts for removal of volatile organic compounds in flue gas by combustion: a review, J. Chem. 2016 (2016) 1–15.
[5] M.S. Kamal, S.A. Razzak, M.M. Hossain, Catalytic oxidation of volatile organic compounds (VOCs)–a review, Atmos. Environ. 140 (2016) 117–134.
[6] K. Everaert, J. Baeyens, Catalytic combustion of volatile organic compounds, J. Hazard. Mater. 109 (2004) 113–139.
[7] S. Bastos, J. Orfao, M. Freitas, M. Pereira, J. Figueiredo, Manganese oxide catalysts synthesized by exotemplating for the total oxidation of ethanol, Appl. Catal. B 93 (2009) 30–37.
[8] S.C. Kim, W.G. Shim, Catalytic combustion of VOCs over a series of manganese oxide catalysts, Appl. Catal. B 98 (2010) 180–185.
[9] V.P. Santos, M.F.R. Pereira, J.J.M. Órfão, J.L. Figueiredo, The role of lattice oxygen on the activity of manganese oxides towards the oxidation of volatile organic compounds, Appl. Catal. B 99 (2010) 353–363.
[10] C. Lahousse, A. Bernier, P. Grange, B. Delmon, P. Papaefthimiou, T. Ioannides, X. Verykios, Evaluation of γ-MnO_2 as a VOC removal catalyst: comparison with a noble metal catalyst, J. Catal. 178 (1998) 214–225.
[11] C. Cellier, V. Ruaux, C. Lahousse, P. Grange, E.M. Gaigneaux, Extent of the participation of lattice oxygen from γ-MnO 2 in VOCs total oxidation: influence of the VOCs nature, Catal. Today 117 (2006) 350–355.
[12] F. Wang, H. Dai, J. Deng, G. Bai, K. Ji, Y. Liu, Manganese oxides with rod-, wire-, tube-, and flower-like morphologies: highly effective catalysts for the removal of toluene, Environ. Sci. Technol. 46 (2012) 4034–4041.
[13] S.C. Kim, The catalytic oxidation of aromatic hydrocarbons over supported metal oxide, J. Hazard. Mater. 91 (2002) 285–299.
[14] G.S.P. Soylu, Z. Ozçelik, I. Boz, Total oxidation of toluene over metal oxides supported on a natural clinoptilolite-type zeolite, Chem. Eng. J. 162 (2010) 380–387.
[15] G.S. Pozan, Effect of support on the catalytic activity of manganese oxide catalyts for toluene combustion, J. Hazard. Mater. 221–222 (2012) 124–130.
[16] D. Chlala, J.-M. Giraudon, N. Nuns, C. Lancelot, R.-N. Vannier, M. Labaki, J.-F. Lamonier, Active Mn species well dispersed on Ca^{2+} enriched apatite for total oxidation of toluene, Appl. Catal. B 184 (2016) 87–95.
[17] R.G. Derwent, M.E. Jenkin, S.M. Saunders, Photochemical ozone creation potentials for a large number of reactive hydrocarbons under European conditions, Atmos. Environ. 30 (1996) 181–199.
[18] R.G. Derwent, M.E. Jenkin, S.M. Saunders, M.J. Pilling, Photochemical ozone creation potentials for organic compounds in northwest Europe calculated with a master chemical mechanism, Atmos. Environ. 32 (1998) 2429–2441.
[19] A.B. Lamb, W.C. Bray, J.C.W. Frazer, The removal of carbon monoxide from air, J. Ind. Eng. Chem. 12 (1920) 213–220.
[20] T. Biemelt, K. Wegner, J. Teichert, M.R. Lohe, J. Martina, J. Grothe, S. Kaskel, Hopcalite nanoparticle catalysts with high water vapour stability forcatalytic oxidation of carbon monoxide, Appl. Catal. B 184 (2016) 208–2015.
[21] M. Krämer, T. Schmidt, K. Stöwe, F. Müller, H. Natter, W.F. Maier, Structural and catalytic aspects of sol–gel derived copper manganese oxides as low-temperature CO oxidation catalyst, Appl. Catal. A 302 (2006) 257–263.
[22] A. Marinoiu, M. Raceanu, C. Cobzaru, C. Teodorescu, D. Marinescu, A. Soare, M. Varlam, Low temperature CO retention using hopcalite catalyst for fuel cell applications, React. Kinet. Catal. Lett. 112 (2014) 37–50.
[23] H. Chen, X. Tong, Y. Li, Mesoporous Cu–Mn Hopcalite catalyst and its performance in low temperature ethylene combustion in a carbon dioxide stream, Appl. Catal. A 370 (2009) 59–65.
[24] X. Li, L. Wang, Q. Xia, Z. Liu, Z. Li, Catalytic oxidation of toluene over copper and manganese based catalysts: effect of water vapor, Catal. Commun. 14 (2011) 15–19.
[25] W.B. Li, W.B. Chu, M. Zhuang, J. Hua, Catalytic oxidation of toluene on Mn–containing mixed oxides prepared in reverse microemulsions, Catal. Today 93–95 (2004) 205–209.
[26] M. Zimowska, A. Michalik-Zym, R. Janik, T. Machej, J. Gurgul, R.P. Socha, J. Podobinski, E.M. Serwicka, Catalytic combustion of toluene over mixed Cu–Mn oxides, Catal. Today 119 (2007) 321–326.
[27] P.A. Wright, S. Natarajan, J.M. Thomas, P.L. Gai-Boyes, Mixed-metal amorphous and spinel phase oxidation catalysts: characterization by x-ray diffraction, x-ray absorption, electron microscopy, and catalytic studies of systems containing copper, cobalt, and manganese, Chem. Mater. 4 (1992) 1053–1065.
[28] P. Porta, G. Moretti, M. Musicanti, A. Nardella, Copper-manganese mixed oxides: formation, characterization and reactivity under different conditions, Solid State Ionics 257 (1993) 63–65.
[29] D.P. Shoemaker, J. Li, R. Seshadri, Unraveling atomic positions in an oxide spinel with two jahn- teller ions: local structure investigation of $CuMn_2O_4$, J. Am. Chem. Soc. 131 (2009) 11450–11457.
[30] M. Kramer, T. Schmidt, K. Stowe, W.F. Maier, Structural and catalytic aspects of sol–gel derived copper manganese oxides as low-temperature CO oxidation catalyst, Appl. Catal. A 302 (2006) 257–263.
[31] E.C. Njagi, C.-H. Chen, H. Genuino, H. Galindo, H. Huang, S.L. Suib, Total oxidation of CO at ambient temperature using copper manganese oxide catalysts prepared by a redox method, Appl. Catal., B. 99 (2010) 103–110.
[32] V.H. Vu, E. Ndzebet, A. Kumar, D. Gilbert, W.C. Bushong, K. Ramaswami, J. Scherer, Copper–manganese mixed oxide cathode material for use in alkaline cells having high capacity, US Patent 7 807 296. (2010).
[33] Q. Liu, L.C. Wang, M. Chen, Y.M. Liu, Y. Cao, H.Y. He, K.N. Fan, Waste-free soft reactive grinding synthesis of high-surface-area copper–manganese spinel oxide catalysts highly effective for methanol steam reforming, Catal. Lett. 121 (2008) 144–150.
[34] D. Rangappa, S. Ohara, M. Umetsu, T. Naka, T. Adschiri, Synthesis, characterization and organic modification of copper manganese oxide nanocrystals under supercritical water, J. Supercrit. Fluids 44 (2008) 441–445.
[35] W.B. Li, W.B. Chu, M. Zhuang, J. Hua, Catalytic oxidation of toluene on Mn–containing mixed oxides prepared in reverse microemulsions, Catal. Today 93–95 (2004) 205–220.
[36] J. Papavasiliou, G. Avgouropoulos, T. Ioannides, In situ combustion synthesis of structured Cu-Ce-O and Cu-Mn-O catalysts for the production and purification of hydrogen, Appl. Catal. B 66 (2006) 168–174.
[37] H. Einaga, A. Kiya, S. Yoshioka, Y. Teraoka, Catalytic properties of copper?manganese mixed oxides prepared by coprecipitation using tetramethylammonium hydroxide, Catal. Sci. Technol. 4 (2014) 3713–3722.
[38] V.P. Santos, M.F.R. Pereira, J.J.M. Orfao, J.L. Figueiredo, Synthesis and characterization of manganese oxide catalysts for the total oxidation of ethyl acetate, Top. Catal. 52 (2009) 470–481.
[39] A.-M. Azad, A. Hedayati, M. Ryd, H. Leion, T. Mattisson, Examining the Cu–Mn–O spinel system as an oxygen carrier in chemical looping combustion, Energy Technol. 1 (2013) 59–69.
[40] F. Kapteijn, A.S. Vanlangeveld, J.A. Moulijn, A. Andreini, M.A. Vuurman, A.M. Turek, J.M. Jehng, I.E. Wachs, Alumina-supported manganese oxide catalysts: I. Characterization: effect of precursor and loading, J. Catal. 150 (1994) 94–104.
[41] J. Papavasiliou, G. Avgouropoulos, T. Ioannides, Combined steam reforming of methanol over Cu–Mn spinel oxide catalysts, J. Catal. 251 (2007) 7–20.
[42] G. Avgouropoulos, T. Ioannides, Selective CO oxidation over CuO-CeO_2 catalysts prepared via the urea–nitrate combustion method, Appl. Catal. A 244 (2003) 155–167.
[43] A.S. Reddy, C. Gopinath, S. Chilukuri, Selective ortho-methylation of phenol with methanol over copper manganese mixed-oxide spinel catalysts, J. Catal. 243 (2006) 278–291.
[44] G. Fierro, S. Morpurgo, M. Lo Jacono, M. Inversi, I. Pettiti, Preparation, characterisation and catalytic activity of Cu-Zn-based manganites obtained from carbonate precursors, Appl. Catal. A 166 (1998) 407–417.
[45] Y. Zhu, W. Zhou, Y. Chen, J. Yu, X. Xu, C. Su, M.O. Tadeí, Z. Shao, Boosting oxygen reduction reaction activity of palladium by stabilizing its unusual oxidation states in perovskite, Chem. Mater. 27 (2015) 3048–3054.
[46] L. Liotta, M. Ousmane, G. Di Carlo, G. Pantaleo, G. Deganello, A. Boreave, A. Giroir-Fendler, Catalytic removal of toluene over Co_3O_4–CeO_2 mixed oxide catalysts: comparison with Pt/Al_2O_3, Catal. Lett. 127 (2009) 270–276.
[47] S.C. Kim, W.G. Shim, Properties and performance of Pd based catalysts for catalytic oxidation of volatile organic compounds, Appl. Catal. B 92 (2009) 429–436.